

Low-energy regeneration and high productivity in a lanthanide–hexacarboxylate framework for high-pressure CO₂–CH₄–H₂ separation†

Yabing He,^{*a} Hiroyasu Furukawa,^b Chuande Wu,^c Michael O’Keeffe,^d Rajamani Krishna^{*e} and Banglin Chen^{*f}

Cite this: *Chem. Commun.*, 2013, **49**, 6773

Received 30th April 2013,
Accepted 6th June 2013

DOI: 10.1039/c3cc43196g

www.rsc.org/chemcomm

A porous lanthanide–organic framework UTSA-62a of a jtt-a topology has been synthesized from a hexacarboxylate and structurally characterized, exhibiting significant potential for use in CO₂–CH₄–H₂ separation (H₂ purification) processes with high productivities and low regeneration costs when operating at high pressure and room temperature.

Metal–organic frameworks (MOFs) or porous coordination polymers have emerged as an exceptionally versatile class of porous materials. By bridging metal centers with appropriate polyfunctional organic linkers, MOF materials can incorporate both tunable pore size/shape and a modifiable pore surface, which offer great promise for a variety of applications, including gas storage, separation, catalysis, chemical sensing and drug delivery.^{1,2}

Research on porous MOFs for carbon capture has mainly focused on the post-combustion CO₂ capture under low pressure, while porous MOFs for the pre-combustion CO₂ capture, and thus H₂ purification under high pressure, have not been extensively explored.³ The well known MgMOF-74 has been comprehensively examined for H₂ purification.^{3a,b} Studies have shown that this MOF does exhibit high separation capacity for H₂ purification; however, the strong interactions between the framework and carbon dioxide lead to the very high regeneration energy costs.

It is highly demanding to develop porous MOF materials which not only exhibit high separation capacity, but also have low regeneration energy costs for such an industrially important process.

We have been pursuing porous MOFs for gas storage and separation over the past several years.⁴ A variety of different metal-containing secondary building units (SBUs) and multicarboxylate organic linkers have been utilized to optimize the pore space for gas storage and to tune the pore/cage sizes for gas separation. The ideal porous MOFs for H₂ purification should have moderately high porosity and weak interactions with carbon dioxide. Herein, we report a new MOF Yb₃O(H₂O)₃(L)(NO₃) (**UTSA-62a**) constructed from [Yb₃O(O₂C)₆] clusters and dendritic hexacarboxylate organic linkers for such a purpose.

The organic linker H₆L was readily synthesized by Suzuki coupling of 1,3,5-tri(3,5-dibromophenyl)benzene and 4-(methoxycarbonyl)phenyl boronic acid followed by hydrolysis and acidification in good yield. A solvothermal reaction between H₆L and Yb(NO₃)₃·5H₂O in *N,N*-dimethylacetamide (DMA) in the presence of a small amount of water at 100 °C afforded colorless block-shaped crystals of **UTSA-62** with an empirical formula of Yb₃O(H₂O)₃(L)(NO₃)·xG (G represents non-coordinated solvent molecules). The structure was determined using single-crystal X-ray diffraction analysis, and the phase purity of the bulk material was confirmed using powder X-ray diffraction (PXRD, Fig. S1, ESI†). Thermogravimetric analysis (TGA) shows that **UTSA-62** can be thermally stable up to 400 °C under a nitrogen atmosphere (Fig. S2, ESI†).

Single-crystal X-ray crystallographic studies reveal that **UTSA-62** crystallizes in a hexagonal space group *P*6̄2c.† The asymmetric unit contains half of the Yb(III) ion, one sixth of the deprotonated ligand, one sixth of the μ₃-oxygen atom and half of the terminal water molecule. The unique Yb1 atom and water oxygen atom O4 lie on a mirror plane, and the deprotonated L ligand and the μ₃-oxygen atom O3 have the crystallographically imposed 3₂ symmetry. Each Yb ion coordinates to six oxygen atoms from four carboxylate groups of L ligands, one terminal water and a μ₃-oxygen atom. Three Yb ions are joined by six carboxylate groups and a μ₃-oxygen atom to form a 6-connected trigonal prismatic SBU [Yb₃O(O₂C)₆]. Each ligand links to six

^a College of Chemistry and Life Sciences, Zhejiang Normal University, Jinhua 321004, China. E-mail: heyabing@gmail.com

^b Department of Chemistry, University of California, Materials Sciences Division, Lawrence Berkeley National Laboratory, Berkeley, California 94720, USA

^c Department of Chemistry, Zhejiang University, Hangzhou 310027, China

^d Department of Chemistry and Biochemistry, Arizona State University, Tempe, Arizona 85287, USA

^e Van’t Hoff Institute for Molecular Sciences, University of Amsterdam, Science Park 904, 1098 XH Amsterdam, The Netherlands. E-mail: r.krishna@mva.nl

^f Department of Chemistry, University of Texas at San Antonio, One UTSA Circle, San Antonio, Texas 78249-0698, USA. E-mail: banglin.chen@utsa.edu; Fax: +1-210-458-7428

† Electronic supplementary information (ESI) available: Synthesis and characterization of the organic linker and **UTSA-62**, PXRD, TGA, NMR, FTIR, sorption isotherms, IAST and breakthrough calculations, fitting parameters for **UTSA-62a**. CCDC 935253. For ESI and crystallographic data in CIF or other electronic format see DOI: 10.1039/c3cc43196g

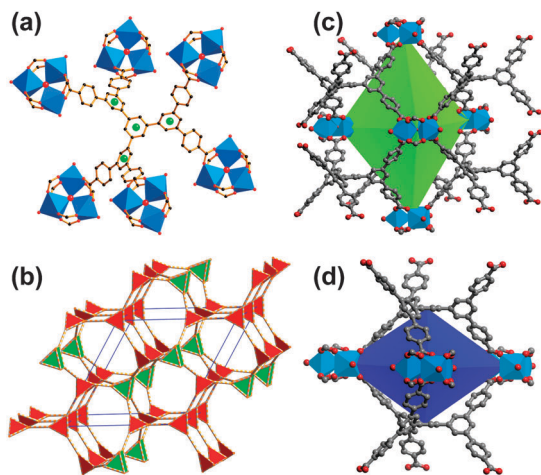


Fig. 1 Single-crystal X-ray structure of **UTSA-62** showing (a) the coordination environment of the organic building block, (b) the framework topology of **jjt-a**, and (c and d) two kinds of polyhedral cages A and B.

SBUs and serves as a 6-connected node (Fig. 1a), generating a (6,6)-connected binodal network structure of **nia** topology.⁵ However, one should recognize the 3-coordinated (3-c) branch points of the hexatopic linker explicitly as there are several distinct ways of replacing the octahedral node of the basic net **nia**. In this case, the derived net is **jjt** shown in Fig. 1b in augmented form (*i.e.* vertices replaced by the vertex figures – triangles and trigonal prisms). There exist two types of trigonal bipyramid cages (cages A and B): cage A is formed by five SBUs as vertices and six ligands as faces with the dimension of *ca.* 15 Å (Fig. 1c), measured by fitting a sphere from the centroid of the cage to the van der Waals surface of its walls; cage B is formed by three SBUs and two ligands with a dimension of *ca.* 14 Å (Fig. 1d). Each cage A is surrounded by three cages B *via* the sharing of tetragonal windows and *vice versa*.

In order to establish the permanent porosity, the as-synthesized sample was guest-exchanged with dry acetone, and then activated using the supercritical CO₂ drying method to remove all solvent molecules. The permanent porosity of activated **UTSA-62a** was confirmed by a N₂ sorption isotherm. As shown in Fig. S3, ESI† the N₂ sorption isotherm shows type-I adsorption behaviour, characteristic of microporous materials with a Brunauer–Emmett–Teller (BET) surface area of 2190 m² g⁻¹ (Fig. S4, ESI†). This is one of the most porous lanthanide–organic frameworks ever reported so far (Table S4, ESI†). Apparently, both the robust [Yb₃O(O₂C)₆] cluster and dendritic hexacarboxylate organic linker play a role in stabilizing the framework. The total pore volume calculated from the maximum amount of N₂ adsorbed is 0.91 cm³ g⁻¹.

Given the high porosity of **UTSA-62a**, we examined the high-pressure CO₂, CH₄ and H₂ adsorption up to 8 MPa using a HPA-100 volumetric high-pressure analyzer. All isotherms show typical type-I behavior with good reversibility (Fig. 2 and Fig. S8, ESI†). The H₂ adsorption isotherm of **UTSA-62a** shows a maximum excess uptake of 4.6 wt% at 3.8 MPa and 77 K (Fig. S8, ESI†). By using the N₂-derived pore volume and the bulk phase density of H₂, the total H₂ uptake at 77 K and 8 MPa was calculated to be 6.3 wt%, which is moderate. At 298 K and 8 MPa, the total H₂ uptake decreases to 1.0 wt% (Fig. 2). **UTSA-62a** shows excess

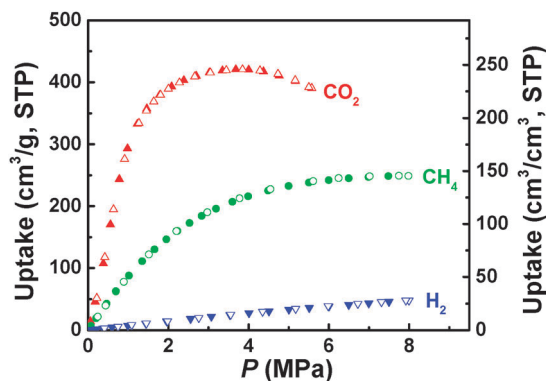


Fig. 2 Excess high-pressure CO₂, CH₄ and H₂ sorption isotherms of **UTSA-62a** at 298 K. Filled and open symbols represent adsorption and desorption data, respectively.

and total CH₄ uptakes of 121 and 139 cm³(STP) per cm³, respectively, at 3.5 MPa and 298 K. The total methane uptake can increase to 189 cm³(STP) per cm³ at 298 K and 8 MPa. The total CO₂ adsorption reaches 47.6 wt% (270 cm³(STP) per cm³) at 298 K and 8 MPa.

The higher CO₂ and CH₄ adsorption capacities of **UTSA-62a** prompted us to examine the potential of **UTSA-62a** for high-pressure CO₂–CH₄–H₂ separation (H₂ purification). In order to establish the feasibility of this separation, we performed IAST (Ideal Adsorbed Solution Theory) and breakthrough calculations for the separation of a 30/20/50 CO₂–CH₄–H₂ gas mixture,⁶ which is likely to be encountered in industrial practice. As shown in Fig. 3a, for a 30/20/50 CO₂–CH₄–H₂ ternary mixture under isothermal conditions at 298 K and a total pressure of 5.0 MPa at the inlet of the adsorber packed with **UTSA-62a**, the hydrogen breaks through earliest, and therefore it is possible to recover pure hydrogen from this 3-component mixture during the adsorption cycle.

We compared the performance of **UTSA-62a** with the widely used zeolites NaX and LTA-5A and the well-examined MOFs MgMOF-74, Cu-TDPAT, Cu-BTC, MIL-101 and UTSA-40a for the high-pressure H₂ purification. The pressure dependent H₂ productivities from 0.1 MPa to 6.0 MPa are shown in Fig. 3b, in which the produced H₂ is more than 99.95% pure. The productivities of **UTSA-62a** are moderately high. In fact, at the highest pressure of 6.0 MPa, the H₂ productivity of **UTSA-62a** is only about 20% lower than those of the best performing MOFs ever reported (MgMOF-74, CuBTC and CuTDPAT) for H₂ purification.

Another very important consideration for such an industrially significant separation is the regeneration cost. Since the isosteric heat of adsorption of CO₂ is the lowest for **UTSA-62a**, as compared to all other adsorbents (Fig. 4), the regeneration cost can be expected to be less than that of MgMOF-74, CuBTC, and CuTDPAT, thus leading to significant energy saving. This reduced regeneration cost could more than offset the slightly low H₂ productivity of **UTSA-62a** relative to MgMOF-74, CuBTC, and CuTDPAT at high pressure. Such low isosteric heats of adsorption of CO₂ are attributed to the highly porous structure and the lack of specific binding sites on the pore surfaces for their interactions with CO₂.

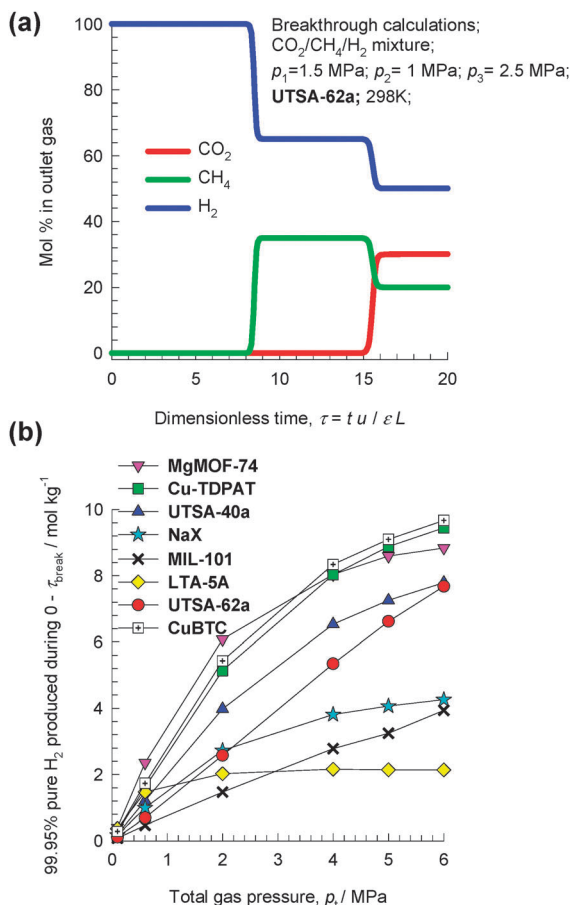


Fig. 3 (a) Transient breakthrough of a 30/20/50 CO₂-CH₄-H₂ mixture in an adsorber packed with **UTSA-62a**, maintained under isothermal conditions at 298 K and 5.0 MPa. (b) Influence of operating pressure on the number of moles of 99.95% pure H₂ produced per kg of adsorbent material from a 30/20/50 CO₂-CH₄-H₂ mixture at 298 K.

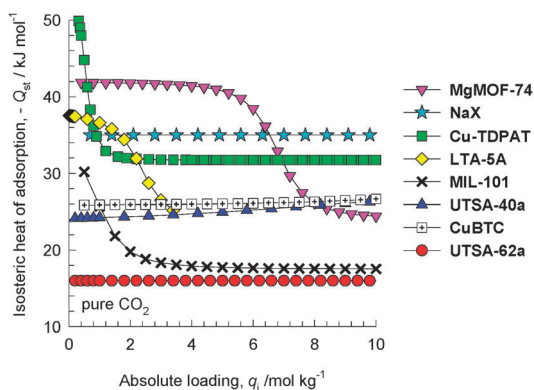


Fig. 4 Comparison of isosteric heats of CO₂ adsorption in **UTSA-62a** with the reported MOFs. The calculations are based on the use of the Clausius-Clapeyron equation.

In summary, we realized a highly porous lanthanide-organic framework **UTSA-62** from a dendritic hexacarboxylate. Both the robust [Yb₃O(O₂C)₆] cluster and dendritic hexacarboxylate

organic linker play crucial roles in stabilizing the framework. The high porosity can secure its high H₂ productivities, while the low isosteric heats of adsorption of CO₂ can minimize the regeneration costs, for H₂ purification at high pressure. **UTSA-62** is a very unique MOF material for this industrially important application in which both the productivities and regeneration costs can be equally considered. Given the richness of MOF chemistry, some even more promising MOF materials (higher productivities and/or lower regeneration costs) for H₂ purification will be targeted in the near future.

Notes and references

† Crystal data for **UTSA-62**: C₁₂₂H₁₈₀N₁₅O₃₉Yb₃, $M = 2999.93$, hexagonal, space group $P62c$, $a = b = 19.848$ Å, $c = 27.853$ Å, $V = 9502.5$ Å³, $Z = 2$, $D_c = 1.048$ g cm⁻³, $\mu(\text{Cu-K}\alpha) = 3.126$ mm⁻¹, $F(000) = 3078$, final $R_1 = 0.0327$ for $I > 2\sigma(I)$, $wR_2 = 0.0866$ for all data, GoF = 1.103. CCDC 935253.

- (a) Y. He, W. Zhou, R. Krishna and B. Chen, *Chem. Commun.*, 2012, **48**, 11813; (b) X. Lin, N. R. Champness and M. Schröder, *Top. Curr. Chem.*, 2010, **293**, 35; (c) J.-R. Li, J. Sculley and H.-C. Zhou, *Chem. Rev.*, 2012, **112**, 869; (d) K. Sumida, D. L. Rogow, J. A. Mason, T. M. McDonald, E. D. Bloch, Z. R. Herm, T.-H. Bae and J. R. Long, *Chem. Rev.*, 2012, **112**, 724; (e) H. Wu, Q. Gong, D. H. Olson and J. Li, *Chem. Rev.*, 2012, **112**, 836; (f) L. Ma, C. Abney and W. Lin, *Chem. Soc. Rev.*, 2009, **38**, 1248; (g) Y. Cui, Y. Yue, G. Qian and B. Chen, *Chem. Rev.*, 2012, **112**, 1126; (h) B. Chen, S. Xiang and G. Qian, *Acc. Chem. Res.*, 2010, **43**, 1115; (i) L. E. Kreno, K. Leong, O. K. Farha, M. Allendorf, R. P. V. Duyne and J. T. Hupp, *Chem. Rev.*, 2012, **112**, 1105; (j) P. Horcajada, R. Gref, T. Baati, P. K. Allan, G. Maurin, P. Couvreur, G. Férey, R. E. Morris and C. Serre, *Chem. Rev.*, 2012, **112**, 1232; (k) S. Horike, S. Shimomura and S. Kitagawa, *Nat. Chem.*, 2009, **1**, 695; (l) R. Banerjee, A. Phan, B. Wang, C. Knobler, H. Furukawa, M. O'Keeffe and O. M. Yaghi, *Science*, 2008, **319**, 939.
- (a) P. Nugent, Y. Belmabkhout, S. D. Burd, A. J. Cairns, R. Luebke, K. Forrest, T. Pham, S. Ma, B. Space, L. Wojtas, M. Eddaoudi and M. J. Zaworotko, *Nature*, 2013, **495**, 80; (b) J. An, S. J. Geib and N. L. Rosi, *J. Am. Chem. Soc.*, 2010, **132**, 38; (c) T. Panda, P. Pachfule, Y. Chen, J. Jiang and R. Banerjee, *Chem. Commun.*, 2011, **47**, 2011; (d) H.-L. Jiang and Q. Xu, *Chem. Commun.*, 2011, **47**, 3351; (e) Q. Lin, T. Wu, S.-T. Zheng, X. Bu and P. Feng, *J. Am. Chem. Soc.*, 2012, **134**, 784; (f) W.-Y. Gao, W. Yan, R. Cai, K. Williams, A. Salas, L. Wojtas, X. Shi and S. Ma, *Chem. Commun.*, 2012, **48**, 8898; (g) J.-P. Zhang and X.-M. Chen, *J. Am. Chem. Soc.*, 2009, **131**, 5516; (h) Y.-X. Tan, Y.-P. He and J. Zhang, *Chem. Commun.*, 2011, **47**, 10647; (i) J. Jia, F. Sun, T. Borjigin, H. Ren, T. Zhang, Z. Bian, L. Gao and G. Zhu, *Chem. Commun.*, 2012, **48**, 6010.
- (a) Z. R. Herm, J. A. Swisher, B. Smit, R. Krishna and J. R. Long, *J. Am. Chem. Soc.*, 2011, **133**, 5664; (b) Z. R. Herm, R. Krishna and J. R. Long, *Microporous Mesoporous Mater.*, 2012, **151**, 481; (c) H. Wu, K. Yao, Y. Zhu, B. Li, Z. Shi, R. Krishna and J. Li, *J. Phys. Chem. C*, 2012, **116**, 16609; (d) Y. He, S. Xiang, Z. Zhang, S. Xiong, C. Wu, W. Zhou, T. Yildirim, R. Krishna and B. Chen, *J. Mater. Chem. A*, 2013, **1**, 2543.
- (a) Y. He, Z. Zhang, S. Xiang, H. Wu, F. R. Fronczek, W. Zhou, R. Krishna, M. O'Keeffe and B. Chen, *Chem.-Eur. J.*, 2012, **18**, 1901; (b) Y. He, Z. Zhang, S. Xiang, F. R. Fronczek, R. Krishna and B. Chen, *Chem. Commun.*, 2012, **48**, 6493; (c) Y. He, S. Xiang, Z. Zhang, S. Xiong, F. R. Fronczek, R. Krishna, M. O'Keeffe and B. Chen, *Chem. Commun.*, 2012, **48**, 10856; (d) Z. Guo, H. Wu, G. Srinivas, Y. Zhou, S. Xiang, Z. Chen, Y. Yang, W. Zhou, M. O'Keeffe and B. Chen, *Angew. Chem., Int. Ed.*, 2011, **50**, 3178.
- M. O'Keeffe, M. A. Peskov, S. J. Ramsden and O. M. Yaghi, *Acc. Chem. Res.*, 2008, **41**, 1782.
- (a) A. L. Myers and J. M. Prausnitz, *AIChE J.*, 1965, **11**, 121; (b) R. Krishna and J. R. Long, *J. Phys. Chem. C*, 2011, **115**, 12941; (c) E. D. Bloch, W. L. Queen, R. Krishna, J. M. Zadrozny, C. M. Brown and J. R. Long, *Science*, 2012, **335**, 1606; (d) Y. He, R. Krishna and B. Chen, *Energy Environ. Sci.*, 2012, **5**, 9107.

Supporting Information for the manuscript

Low-energy regeneration and high productivity in a lanthanide-hexacarboxylate framework for high-pressure CO₂/CH₄/H₂ separation

5 Yabing He,^a Hiroyasu Furukawa,^b Chuande Wu,^c Michael O'Keeffe,^d Rajamani Krishna,^{*e} Banglin Chen^{*f}

^a *College of Chemistry and Life Sciences, Zhejiang Normal University, Jinhua 321004, China*

^b *Department of Chemistry, University of California and Molecular Foundry, Materials Sciences Division, Lawrence Berkeley National Laboratory, Berkeley, California 94720, USA*

^c *Department of Chemistry, Zhejiang University, Hangzhou 310027, China*

^d *Department of Chemistry and Biochemistry, Arizona State University, Tempe, Arizona 85287, USA*

^e *Van 't Hoff Institute for Molecular Sciences, University of Amsterdam, Science Park 904, 1098 XH Amsterdam, The Netherlands; E-mail: r.krishna@nva.nl*

^f *Department of Chemistry, University of Texas at San Antonio, One UTSA Circle, San Antonio, Texas 78249-0698, USA. Fax: (+1)-210-458-7428; E-mail: banglin.chen@utsa.edu*

20

25

30

General remarks

All starting materials and reagents for synthesis were commercially available and used as received. ^1H NMR and ^{13}C NMR spectra were recorded on a Varian Mercury 300 MHz spectrometer. Tetramethylsilane (TMS) and deuterated solvents were used as internal standards in ^1H NMR and ^{13}C NMR experiments, respectively. Fourier transform infrared (FTIR) spectra were recorded using a Bruke Vector 22 spectrometer between 650 cm^{-1} and 4000 cm^{-1} . Thermogravimetric analyses (TGA) were carried out using a Shimadzu TGA-50 thermal analyzer with a heating rate of $5\text{ }^\circ\text{C min}^{-1}$ in a flowing nitrogen atmosphere. Powder X-ray diffraction (PXRD) patterns were recorded on a Rigaku Ultima IV X-ray diffractometer operating at 40 kV and 44 mA with a scan rate of 1.0 deg min^{-1} , using Cu-K_α radiation. Low-pressure gas adsorption experiments were carried out on a Quantachrome AUTOSORB-1 automatic volumetric gas adsorption analyzer. High-pressure gas adsorption isotherms were measured using the static volumetric method in an HPA-100 from the VTI Corporation (currently Particulate Systems). To obtain the excess adsorption isotherms, all data points were corrected for buoyancy and the thermal gradient that arises between the balance and the sample bucket. Ultra-high-purity grade CH_4 , H_2 (99.999% purity) and CO_2 (99.995% purity) gases were used throughout the high-pressure adsorption experiments. Before the gas sorption measurements were performed, the as-synthesized samples were guest-exchanged with dry acetone, and then activated using supercritical CO_2 drying method to remove all solvent molecules. Briefly, the acetone-containing sample was placed in the chamber in a Tousimis Samdri PVT-3D critical point dryer, and acetone was completely exchanged with liquid CO_2 . The CO_2 was slowly vented from the chamber, yielding the activated material **UTSA-62a**.

Single-crystal X-ray crystallography

The crystal data were collected on an Oxford Xcalibur Gemini Ultra diffractometer with an Atlas detector. The data were collected using graphite-monochromatic enhanced ultra Cu radiation ($\lambda = 1.54178\text{ \AA}$) at 293 K. The datasets were corrected by empirical absorption correction using spherical harmonics, implemented in the SCALE3 ABSPACK scaling algorithm. The structure was solved by direct methods and refined by full matrix least-squares methods with the SHELX-97 program package. The solvent molecules in the compound are highly disordered. The SQUEEZE subroutine of the PLATON software suit was used to remove the scattering from the highly disordered guest molecules.

The resulting new files were used to further refine the structures. The H atoms on C atoms were generated geometrically.

Fitting of pure-component isotherms

The pure component isotherm data for CO₂, CH₄ and H₂ in **UTSA-62a** do not demonstrate any inflection characteristics and the single-site Langmuir model

$$q = \frac{q_{A,sat} b_A p}{1 + b_A p}$$

with T -dependent parameters b_A

$$b_A = b_{A0} \exp\left(\frac{E_A}{RT}\right) \quad (1)$$

provides an adequately good representation of the absolute component loadings. The isotherm parameters are provided in *Table S1*. The pure component isotherm data for H₂ in **UTSA-62a** is determined at 298 K, and the single-site Langmuir parameters are provided in *Table S2*.

Calculations of adsorption selectivity

The selectivity of preferential adsorption of component 1 over component 2 in a mixture containing 1 and 2, perhaps in the presence of other components too, can be formally defined as

$$S_{ads} = \frac{q_1/q_2}{p_1/p_2} \quad (2)$$

In equation (2), q_1 and q_2 are the *absolute* component loadings of the adsorbed phase in the mixture. In all the calculations to be presented below, the calculations of S_{ads} are based on the use of the Ideal Adsorbed Solution Theory (IAST) of Myers and Prausnitz.¹ These calculations are carried out using the pure component isotherm fits of absolute component loadings.

For H₂ purification, two selectivity metrics are important: CO₂/H₂, and CH₄/H₂ because both impurities CO₂, and CH₄ need to be preferentially adsorbed to obtain H₂ with the desired purity levels. *Figure S10a* presents the IAST calculations of the CO₂/H₂ adsorption selectivity in the ternary mixture, defined by equation (2). The calculations are for a 30/20/50 CO₂/CH₄/H₂ ternary gas mixture that is typically encountered in H₂ purification processes. The highest selectivities are obtained with **MgMOF-74**, **LTA-5A** and **NaX**. The impurity with the lowest adsorption strength is CH₄, and for H₂ purification, the CH₄/H₂ selectivity is also of importance. The CH₄/H₂ selectivities are compared in *Figure S10b*. For pressures exceeding 1 MPa, the CH₄/H₂ selectivities are highest for **CuBTC**, **MgMOF-74**, **UTSA-40a**, and **UTSA-62a**.

The performance of a PSA unit is dictated not only by the adsorption selectivity but also by the capacity to adsorb both CO₂, and CH₄. Generally speaking, higher capacities are desirable because the adsorber bed can be run for longer lengths of time before the need for regeneration arises. The sum of the component loadings of CO₂ and CH₄ in the mixture, is an appropriate measure of the capacity. *Figure S11* presents data on the IAST calculations of the (CO₂ + CH₄) uptake capacities *per* kg of adsorbent. For pressures exceeding 1 MPa, the highest uptake capacities are for **MgMOF-74**, **CuBTC**, **CuTDPAT**. At the highest pressure of 6 MPa, which is likely to be encountered in H₂ purification, we note that **UTSA-62a** has the highest uptake capacity. The lowest uptake capacities are for the traditionally used zeolites **LTA-5A** and **NaX**; this is due to the fact that **LTA-5A** and **NaX** have pore volumes of 0.25 cm³/g and 0.28 cm³/g, respectively, significantly lower than those of the MOFs considered here. We will see later that the capacity of **LTA-5A** and **NaX** for (CO₂ + CH₄) uptake becomes limiting for high-pressure operations in fixed bed adsorbers. Put another way, MOFs with “open” structures are especially attractive for high pressure separations. **MgMOF-74** is the most unusual MOF because it has a combination of both high selectivities and high capacities.

15

Packed bed adsorber breakthrough simulation methodology

It is now well recognized that the separation characteristics of a PSA unit is dictated by a combination of adsorption selectivity and capacity. For a rational choice of adsorbents for mixture separation at high pressures, we need to have a proper method of evaluation that combines the *selectivity* and *capacity* metrics in a manner that is a true reflection of the separation performance of a fixed bed adsorber, shown schematically in *Figure S9*. In order to obtain a realistic appraisal of the separation characteristics of various MOFs for H₂ purification, we perform transient breakthrough calculations. The methodology followed is identical to the ones described in detail in earlier works.²⁻¹³ Experimental validation of the breakthrough simulation methodology is also available in the published literature.^{3,9,14}

The following parameter values were used in the simulations to be reported below: length of packed bed $L = 0.1$ m; bed voidage $\varepsilon = 0.4$; interstitial gas velocity $v = 0.1$ m/s (at inlet). When comparing different materials, the fractional voidage is held constant at $\varepsilon = 0.4$. This implies the volumes of adsorbents used in the fixed bed are the same for all adsorbent materials. The total mass of the adsorbents used is governed by the framework density.

30

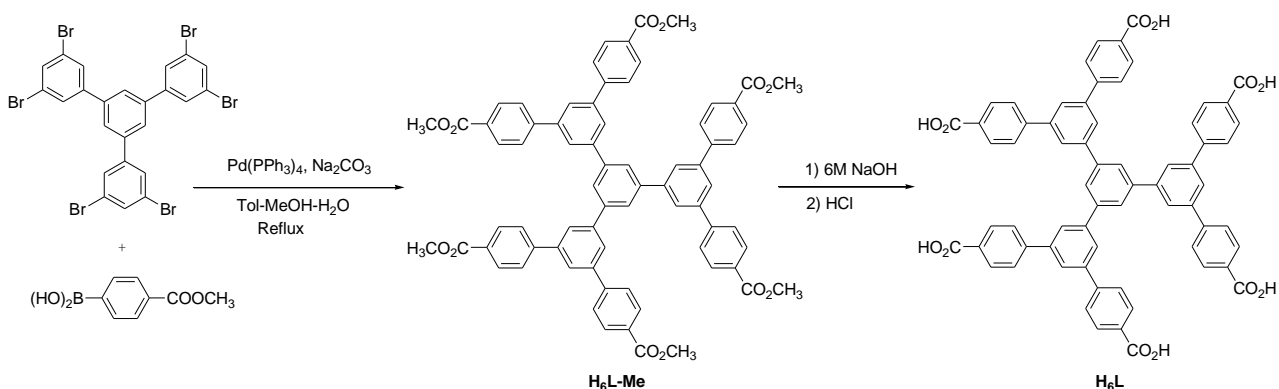
Ternary 30/20/50 CO₂/CH₄/H₂ breakthrough simulations

For industrial production of H₂, impurities such as CO₂, and CH₄ need to be reduced to extremely low levels, typically lower than 500 ppm. A comparison of the breakthrough characteristics of different adsorbents is presented in *Figure S12*. When the composition in the exit gas reaches a certain desired purity level, the adsorption cycle needs to be terminated and the contents of the bed regenerated. Longer breakthrough times are desirable because this reduces the frequency of regeneration. We choose the purity level to be 500 ppm (CO₂ + CH₄) in outlet gas, which is typical of industrial requirements. When this purity level is reached, the corresponding dimensionless breakthrough time, τ_{break} , can be determined.

To demonstrate how the choice of the best material alters with operating pressures, we carried out a series of breakthrough calculations for all seven MOFs for pressures ranging from 0.1 MPa to 6.0 MPa. *Figure S13* shows the influence of the total operating pressure on dimensionless breakthrough times, τ_{break} . Generally speaking, the value of τ_{break} decreases for most materials with increasing pressure. This is due to limitations in the capacities with increasing pressure. For MOFs such as **UTSA-62a**, **UTSA-40a**, and **MIL-101**, there is no capacity limitation for this pressure range, and there is hardly any decrease in τ_{break} .

Figure 3b in the paper presents data on the number of moles of H₂ produced, containing less than 500 ppm impurities (CO₂ + CH₄), produced *per* kg of adsorbent material during the time interval 0 – τ_{break} ; this quantity is obtained from a material balance across the fixed bed adsorber. The productivities of **CuTDPAT** and **CuBTC** are remarkably similar; this is not really surprising because these two MOFs have similar pore topologies, selectivities, and capacities. The productivities of **NaX** and **LTA-5A** tend to reach plateau values for pressures exceeding 2 MPa; this is a direct consequence of the capacity limitations of these zeolites. At the other end of the spectrum, the two MOFs with the high pore volumes **UTSA-62a** and **UTSA-40a** show a steep increase in productivity with increasing pressure. Their performance is poor at low pressures but improves significantly at high pressures. For pressures exceeding 4 MPa, typical of hydrogen purification, the hierarchy of productivities is **MgMOF-74** \approx **CuTDPAT** \approx **CuBTC** > **UTSA-40a** > **UTSA-62a** > **NaX** > **MIL-101** > **LTA-5A**. Remarkably, at the highest pressure of 6 MPa, the H₂ productivity of **UTSA-62a** is only about 20% lower than that of **MgMOF-74**, **CuBTC**, and **CuTDPAT**. Since the isosteric heat of adsorption of CO₂ is the lowest for **UTSA-62a**, as compared to all other adsorbents (see Figure 4 in the paper), the regeneration costs can be expected to be less than that of **MgMOF-74**, **CuBTC**, and **CuTDPAT**. This reduced regeneration costs could more than off-set the lower H₂ productivity of **UTSA-62a**.

Synthesis and characterization of the organic building block



Scheme S1. Synthetic route to the organic building block H₆L.

To a mixture of 1,3,5-tri(3,5-dibromophenyl)benzene (2.00 g, 2.56 mmol), 4-(methoxycarbonyl)phenylboronic acid (3.23 g, 17.95 mmol, Alfa), anhydrous Na₂CO₃ (6.52 g, 61.56 mmol, Alfa) and Pd(PPh₃)₄ (0.89 g, 0.77 mmol, Aldrich) were added degassed toluene-methanol-water mixed solvents (120/60/60 mL). The resulting reaction mixture was stirred for 72 h under reflux under
10 a nitrogen atmosphere. After removal of the solvents, the residue was extracted with CHCl₃ (100 mL × 4), washed with brine (100 mL), dried over anhydrous MgSO₄, filtered, and concentrated in vacuum. The residue was washed with ethyl acetate to give hexamethyl ester intermediate as a pure white solid (2.19 g, 1.97 mmol) in 77% yield, which was hydrolyzed with 6 M NaOH to afford the title compound
15 in quantitative yield. ¹H NMR (DMSO-*d*₆, 300.0 MHz) δ (ppm): 13.031 (s, br, 6H), 8.334 (s, 3H), 8.209 (d, *J* = 1.5 Hz, 6H), 8.018-8.089 (m, 27H); ¹³C NMR (DMSO-*d*₆, 75.4 MHz) δ (ppm): 166.968, 143.964, 142.032, 141.632, 140.455, 129.764, 127.418, 126.164, 124.937; FTIR (neat, cm⁻¹): 1681, 1606, 1587, 1567, 1512, 1381, 1226, 1177, 1102, 1015, 844, 766, 696, 680.

Synthesis and characterization of UTSA-62

20 A mixture of the organic building block H₆L (10.0 mg, 9.7 μmol) and Yb(NO₃)₃ · 5H₂O (25.0 mg, 55.7 μmol, Aldrich) was dispersed in a mixed solvent (*N,N*-dimethylacetamide (DMA)/H₂O: 1.5 mL/0.1 mL) in a disposable scintillation vial (20 mL) under sonication. The vial was capped and heated at 100 °C for 72 h. The block shaped crystals were collected in 56% yield. FTIR (neat, cm⁻¹): 1624, 1597, 1585, 1552, 1504, 1392, 1306, 1261, 1184, 1012, 860, 787, 708.

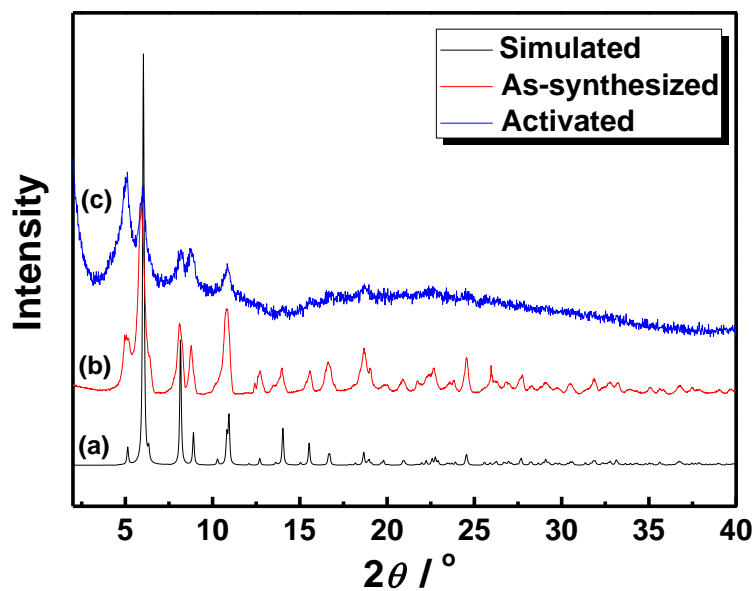


Figure S1. PXRD patterns of as-synthesized **UTSA-62** (b) and activated **UTSA-62a** (c) along with the simulated XRD pattern from the single-crystal X-ray structure (a).

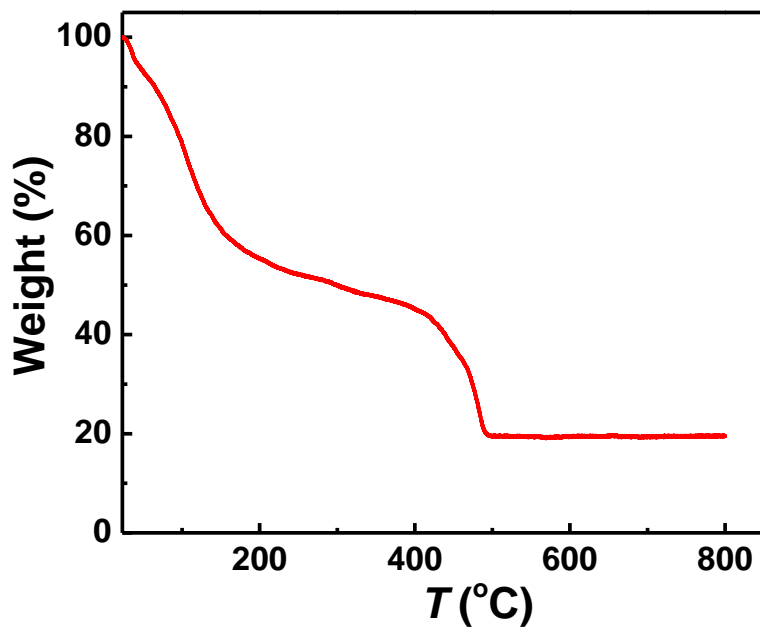


Figure S2. TGA curve of as-synthesized **UTSA-62a** in a flowing N_2 atmosphere.

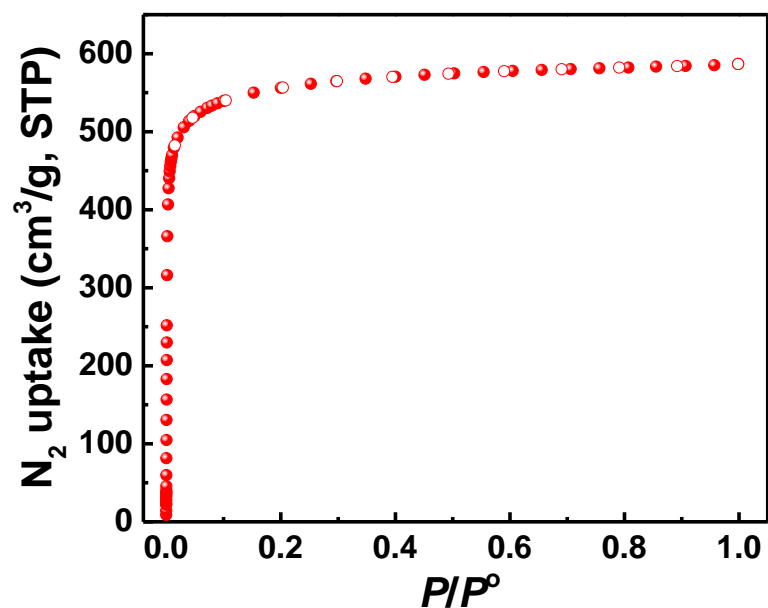
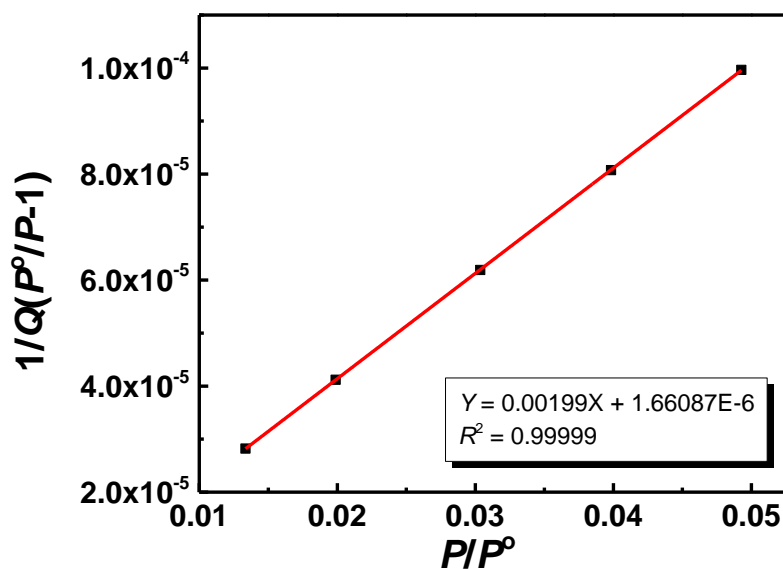


Figure S3. N₂ sorption isotherm of **UTSA-62a** at 77 K. Filled and open symbols represent adsorption and desorption data, respectively.



5
$$S_{\text{BET}} = 1 / (0.00199 + 1.68087 \times 10^{-6}) / 22414 \times 6.023 \times 10^{23} \times 0.162 \times 10^{-18} = 2186 \text{ m}^2/\text{g}$$

Figure S4. BET plot of **UTSA-62a**. Only the range below $P/P^0 = 0.05$ satisfies the first consistency criterion for applying the BET theory.

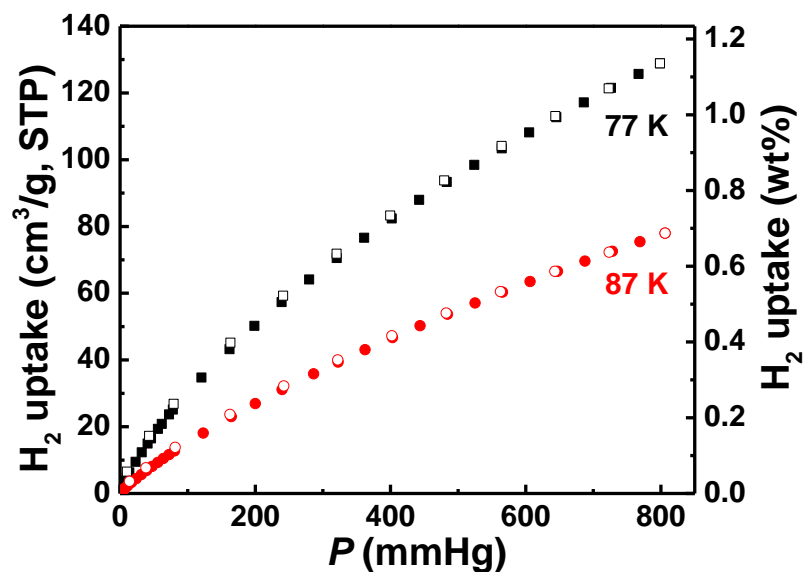
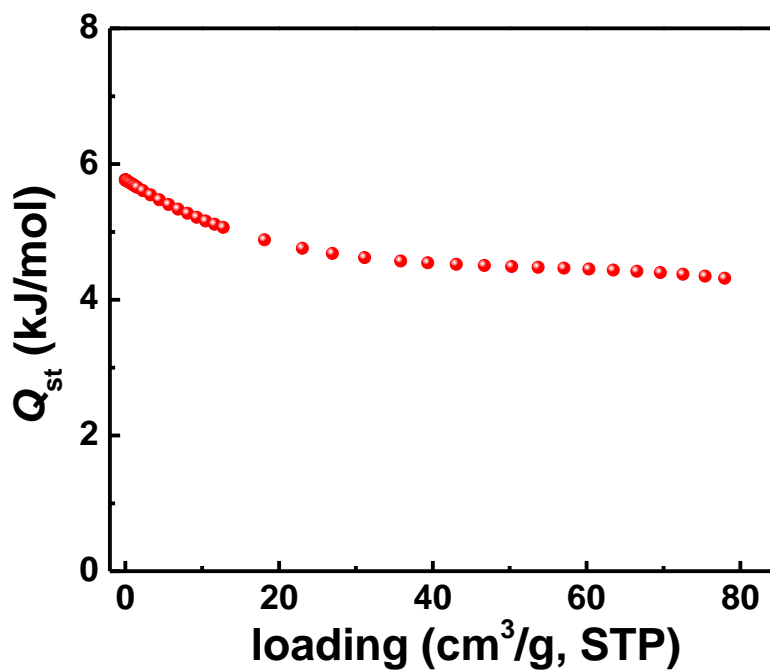


Figure S5. H₂ sorption isotherms of UTSA-62a at 77 K (black) and 87 K (red). Filled and open symbols represent adsorption and desorption data, respectively.



5

Figure S6. The isosteric heat of H₂ adsorption in UTSA-62a.

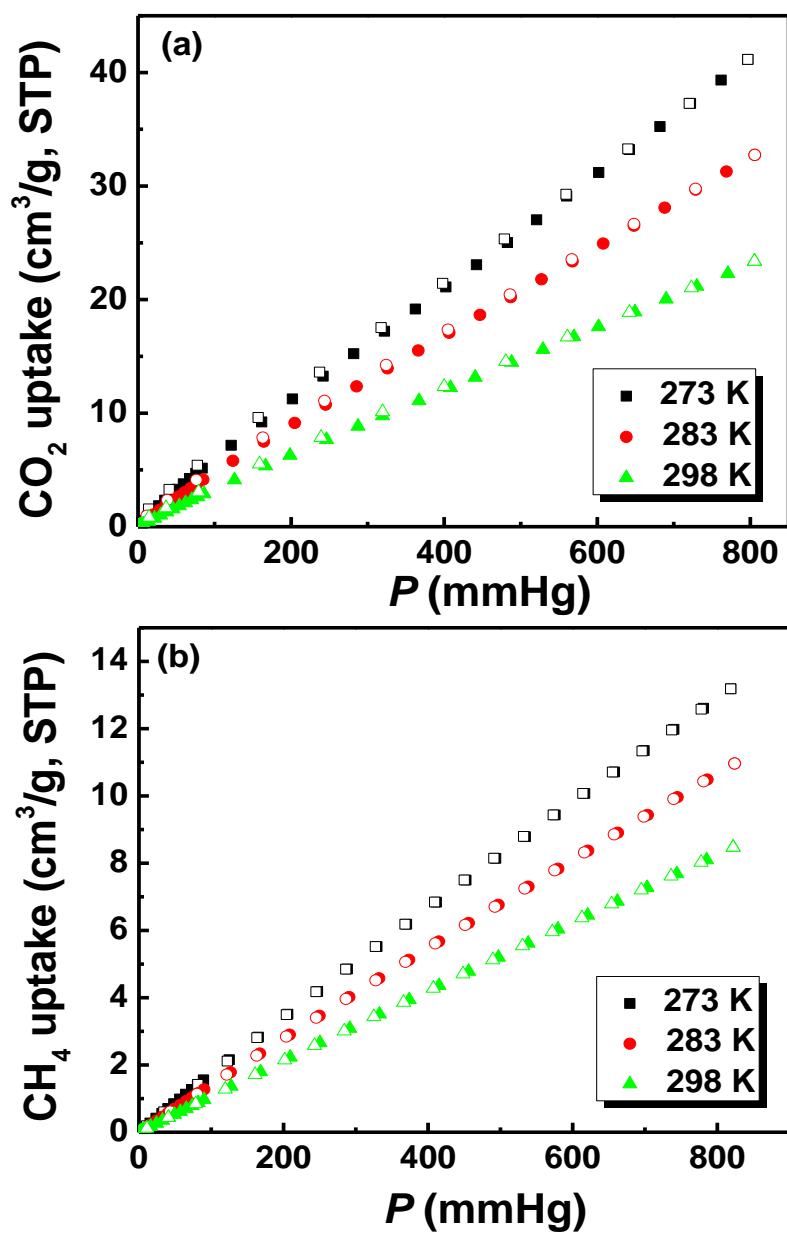


Figure S7. CO₂ (a) and CH₄ (b) sorption isotherms of UTSA-62a at 273 K (black), 283 K (red) and 298 K (green). Filled and open symbols represent adsorption and desorption data, respectively.

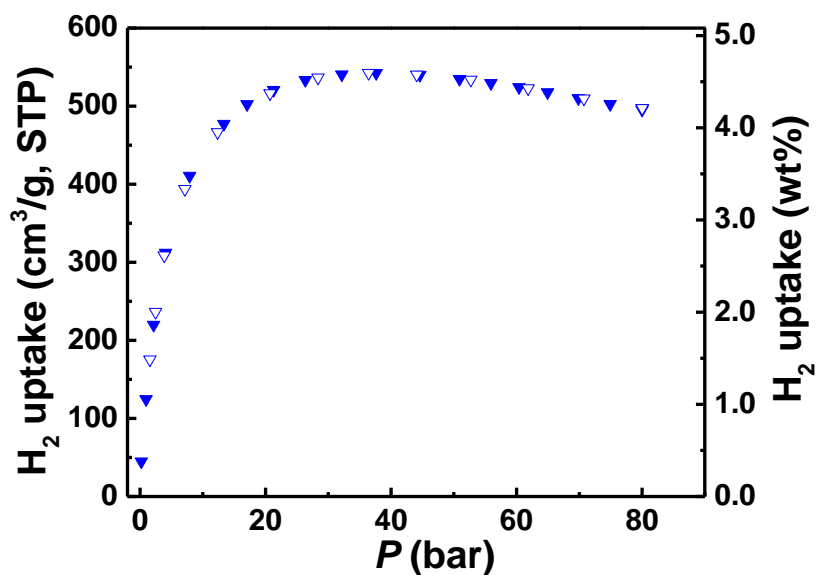


Figure S8. Excess high-pressure H₂ sorption isotherm of **UTSA-62a** at 77 K. Filled and open symbols represent adsorption and desorption data, respectively.

5

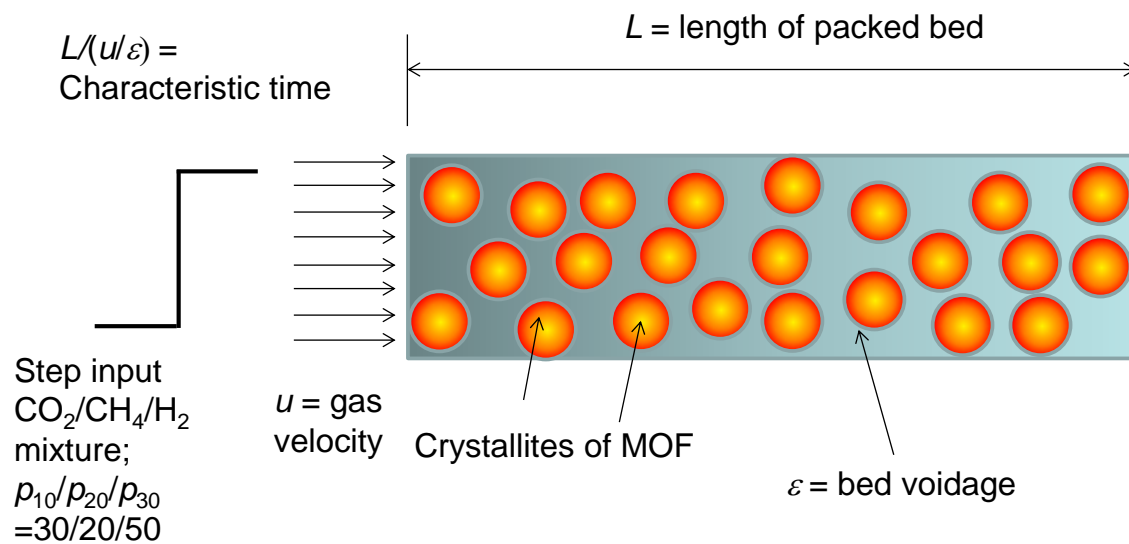


Figure S9. Schematic of a packed bed adsorber.

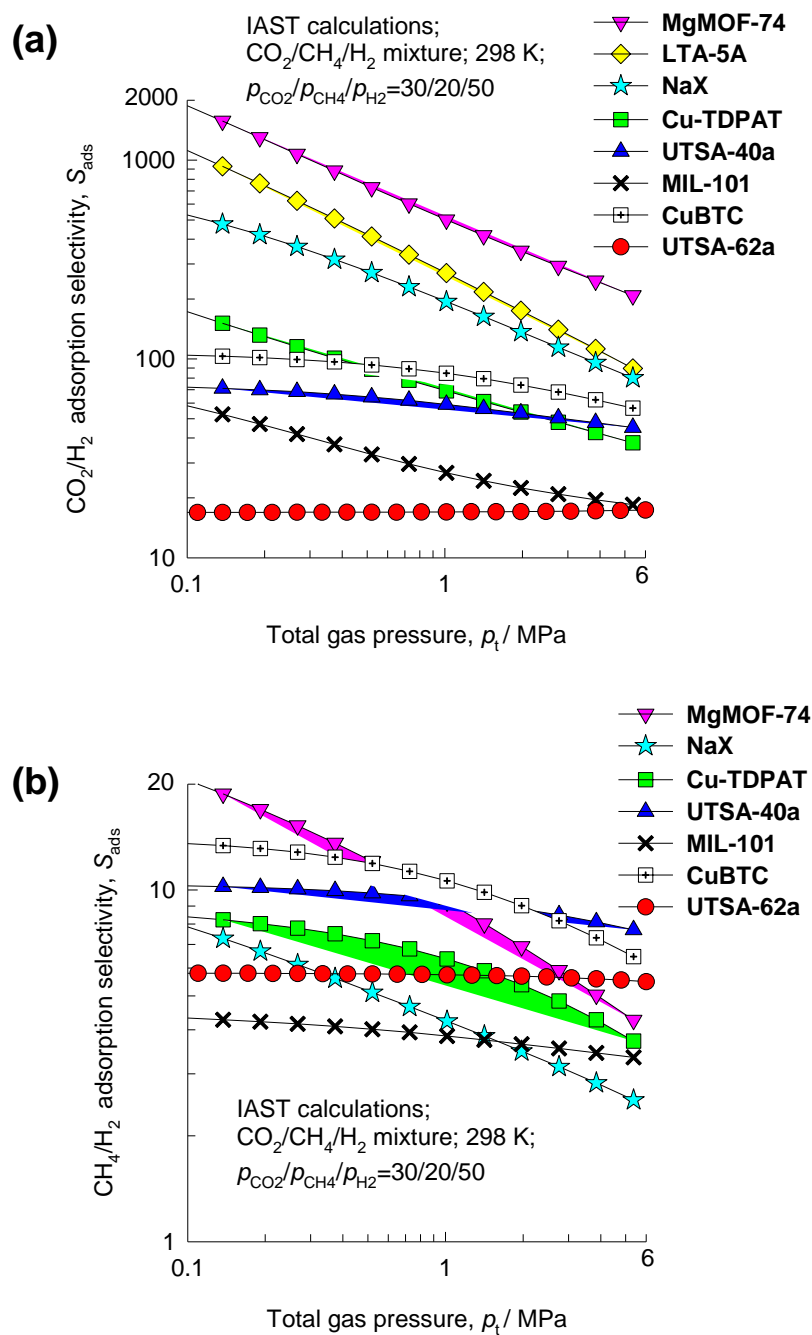


Figure S10. Calculations using IAST for (a) CO₂/H₂ and (b) CH₄/H₂ adsorption selectivities for a 30/20/50 CO₂/CH₄/H₂ ternary gas mixture maintained at isothermal conditions at 298 K.

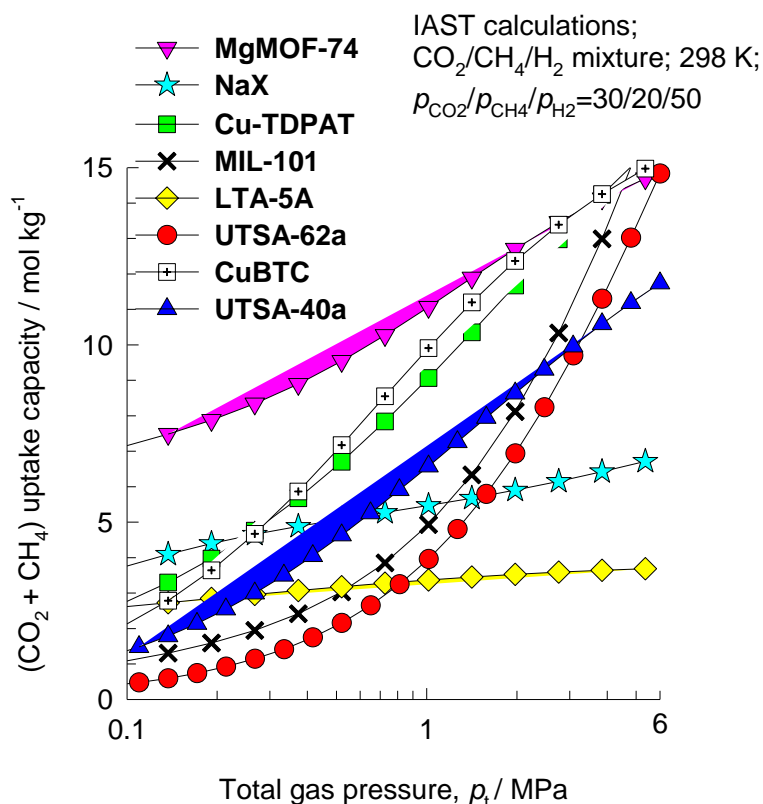
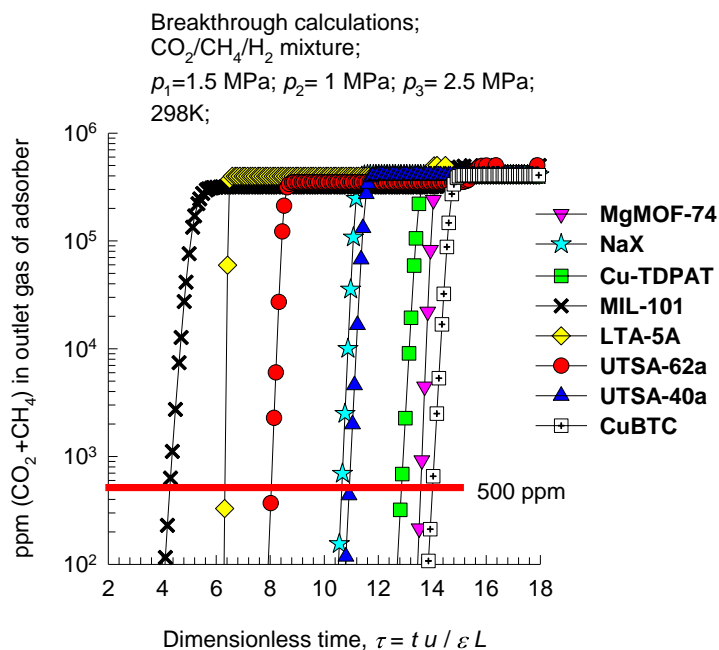


Figure S11. Calculations using IAST for (CO₂ + CH₄) uptake capacity, expressed as moles *per* kg of adsorbent, in equilibrium with a 30/20/50 CO₂/CH₄/H₂ ternary gas mixture maintained at isothermal conditions at 298 K.



5

Figure S12. Ppm (CO₂+CH₄) in outlet gas as a function of the dimensionless time, τ , for various adsorbent materials. The total operating pressure for the data corresponds to 5.0 MPa.

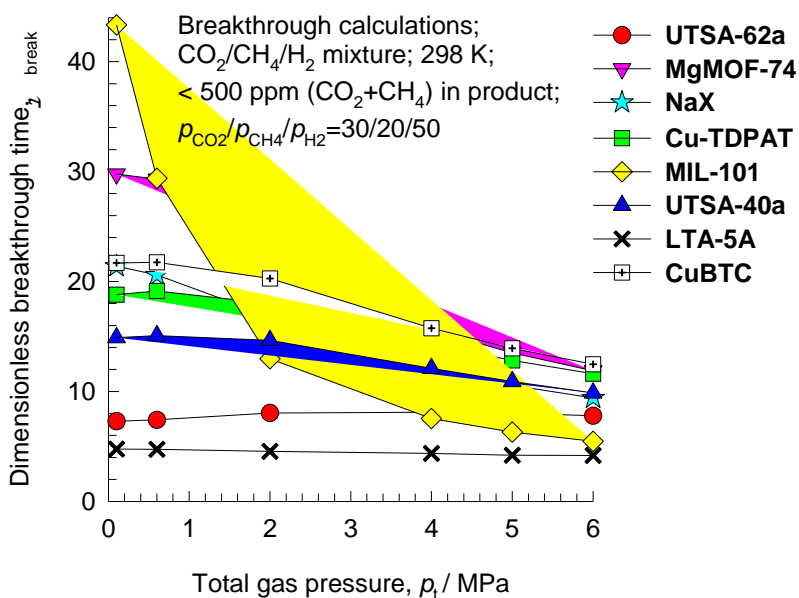


Figure S13. Influence of the total operating pressure, p_t , on dimensionless breakthrough time, τ_{break} .

5

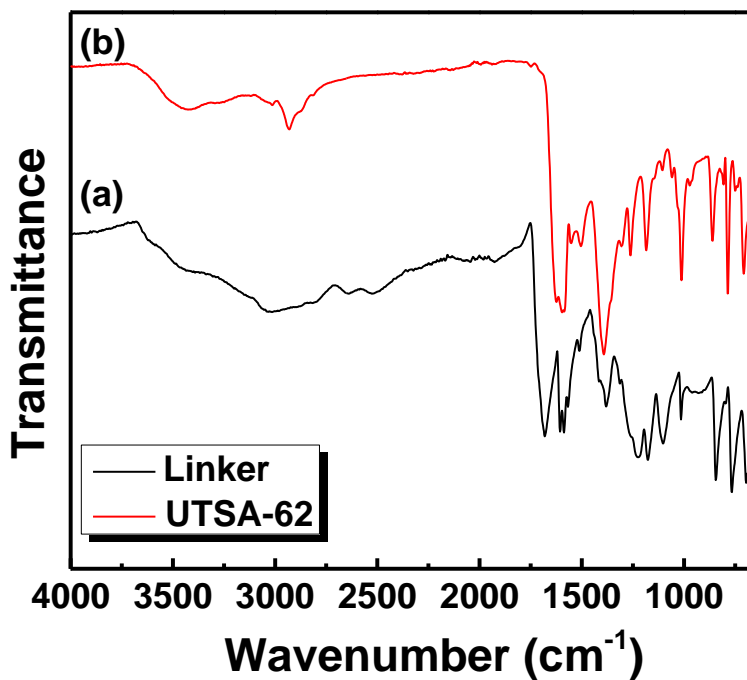


Figure S14. FTIR spectra of the organic linker H₄L (a), and as-synthesized UTSA-62 (b).

10

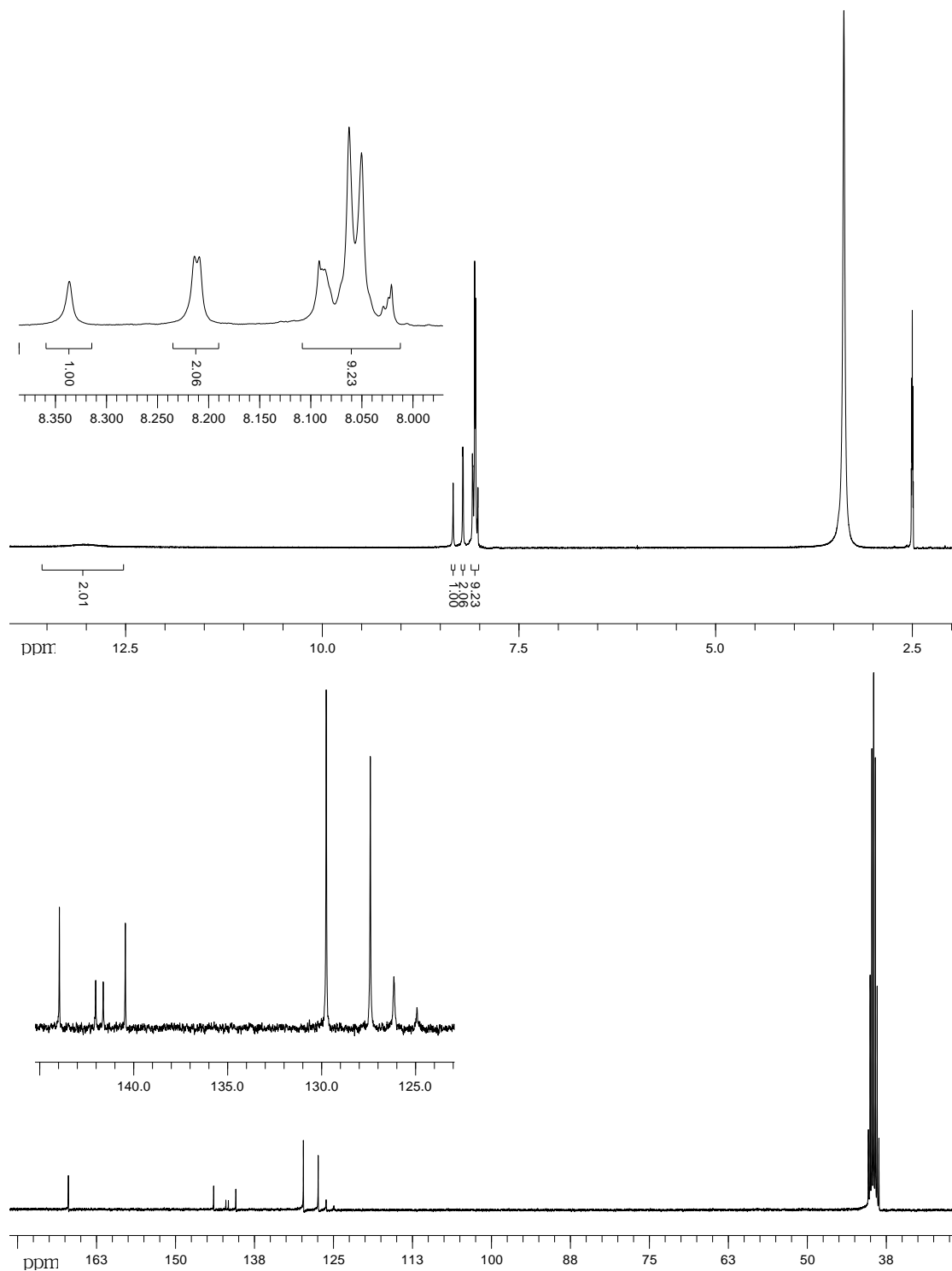


Figure S15. ¹H NMR (DMSO-*d*₆, 300.0 MHz) and ¹³C NMR (DMSO-*d*₆, 75.4 MHz) spectra of the organic building block H₆L.

Table S1. Single-site Langmuir fitting parameters for adsorption of CO₂ and CH₄ in **UTSA-62a**. The fits are based on low-pressure isotherm data measured at 273 K, 283 K, and 298 K, and high-pressure isotherm data at 298 K.

	$q_{A,sat}$ (mol kg ⁻¹)	b_{A0} (Pa ⁻¹)	E_A (kJ mol ⁻¹)
CO ₂	38	4.96×10^{-10}	16
CH ₄	30	2.24×10^{-9}	10.2

Table S2. Single-site Langmuir fitting parameters for pure H₂ isotherms in **UTSA-62a**. The fit is for a temperature of 298 K.

	$q_{A,sat}$ (mol kg ⁻¹)	b_A (Pa ⁻¹)
H ₂	35	2.03×10^{-8}

Table S3. Structural data on different adsorbents evaluated in this study for comparison purposes. The data for **MgMOF-74** and **NaX** are from Herm et al.¹⁵ and Krishna and Long.⁴ The data for **MIL-101** are taken from Chowdhury et al.¹⁶ The data for **Cu-TDPAT** are from Wu et al.³ The data for **LTA-5A** are from Pakseresht et al.¹⁷ and Sircar and Golden.¹⁸ The data for **UTSA-40a** are from He et al.¹⁹

MOFs	Surface area (m ² g ⁻¹)	Pore volume (cm ³ g ⁻¹)	Framework density (kg m ⁻³)
MgMOF-74	1800	0.573	905
MIL-101	2674	1.38	440
CuBTC	2097	0.848	879
Cu-TDPAT	1938	0.93	782
NaX zeolite	950	0.280	1421
LTA-5A	450	0.250	1508
UTSA-40a	1630	0.654	827
UTSA-62a	2186	0.9077	584.3

Table S4. BET surface areas of lanthanide-organic frameworks.

MOF	Formula	BET (m ² g ⁻¹)	Reference
	KHo(C ₂ O ₄) ₂	69.1	20
	Gd ₂ (imidc) ₂	372	21
	Na ₆ Eu(L) ₄ Cl	426	22
	Er ₂ (PDC) ₃	427	23
	Gd ₂ (FDA) ₃	438	24
	Eu ₂ (1,3-BDC) ₃	502	25
	Yb(BPT)	515.6	26
	Gd(BTC)	585	27
	Dy(BTC)	655	28
	Y ₂ (PDC) ₃	676	23
MIL-103	Tb(BTB)	730-930	29
PCN-17(Dy)	Dy ₄ (TATB) _{8/3} (SO ₄) ₂	738	30
	Nd(TPO)	793	31
PCN-17(Yb)	Yb ₄ (TATB) _{8/3} (SO ₄) ₂	820	32
	La(BTB)	1014	33
	Y(BTC)	1080	34
	Tb(TATB)	1783	35
UTSA-62a	Yb ₃ O(H ₂ O) ₃ (L)(NO ₃)	2186	This work

References

1. Myers, A. L.; Prausnitz, J. M., Thermodynamics of mixed-gas adsorption. *AIChE J.* **1965**, *11*, 121-127.
2. Herm, Z. R.; Krishna, R.; Long, J. R., CO₂/CH₄, CH₄/H₂ and CO₂/CH₄/H₂ separations at high pressures using Mg₂(dobdc). *Microporous Mesoporous Mater.* **2012**, *151*, 481-487.
3. Wu, H.; Yao, K.; Zhu, Y.; Li, B.; Shi, Z.; Krishna, R.; Li, J., Cu-TDPAT, an rht-Type Dual-Functional Metal-Organic Framework Offering Significant Potential for Use in H₂ and Natural Gas Purification Processes Operating at High Pressures. *J. Phys. Chem. C* **2012**, *116*, 16609-16618.
4. Krishna, R.; Long, J. R., Screening Metal-Organic Frameworks by Analysis of Transient Breakthrough of Gas Mixtures in a Fixed Bed Adsorber. *J. Phys. Chem. C* **2011**, *115*, 12941-12950.
5. Krishna, R.; Baur, R., Modelling issues in zeolite based separation processes. *Sep. Purif. Technol.* **2003**, *33*, 213-254.
6. Krishna, R.; Baur, R., Diffusion, Adsorption and Reaction in Zeolites: Modelling and Numerical Issues. <http://www.science.uva.nl/research/cr/zeolite/>, University of Amsterdam, Amsterdam, 11 November **2003**.

7. Krishna, R., Adsorptive separation of CO₂/CH₄/CO gas mixtures at high pressures. *Microporous Mesoporous Mater.* **2012**, *156*, 217-223.
8. Krishna, R.; van Baten, J. M., A comparison of the CO₂ capture characteristics of zeolites and metal-organic frameworks. *Sep. Purif. Technol.* **2012**, *87*, 120-126.
9. He, Y.; Krishna, R.; Chen, B., Metal-Organic Frameworks with Potential for Energy-Efficient Adsorptive Separation of Light Hydrocarbons. *Energy Environ. Sci.* **2012**, *5*, 9107-9120.
10. He, Y.; Zhang, Z.; Xiang, S.; Fronczek, F. R.; Krishna, R.; Chen, B., A Microporous Metal-Organic Framework for Highly Selective Separation of Acetylene, Ethylene and Ethane from Methane at Room Temperature. *Chem. Eur. J.* **2012**, *18*, 613-619.
11. He, Y.; Zhang, Z.; Xiang, S.; Fronczek, F. R.; Krishna, R.; Chen, B., A robust doubly interpenetrated metal-organic framework constructed from a novel aromatic tricarboxylate for highly selective separation of small hydrocarbons. *Chem. Commun.* **2012**, *48*, 6493-6495.
12. He, Y.; Zhang, Z.; Xiang, S.; Wu, H.; Fronczek, F. R.; Zhou, W.; Krishna, R.; O'Keeffe, M.; Chen, B., High Separation Capacity and Selectivity of C₂ Hydrocarbons over Methane within a Microporous Metal-Organic Framework at Room Temperature. *Chem. Eur. J.* **2012**, *18*, 1901-1904.
13. He, Y.; Zhou, W.; Krishna, R.; Chen, B., Microporous metal-organic frameworks for storage, and separation of small hydrocarbons. *Chem. Commun.* **2012**, *48*, 11813-11831.
14. Bloch, E. D.; Queen, W. L.; Krishna, R.; Zadrozny, J. M.; Brown, C. M.; Long, J. R., Hydrocarbon Separations in a Metal-Organic Framework with Open Iron(II) Coordination Sites. *Science* **2012**, *335*, 1606-1610.
15. Herm, Z. R.; Swisher, J. A.; Smit, B.; Krishna, R.; Long, J. R., Metal-Organic Frameworks as Adsorbents for Hydrogen Purification and Pre-Combustion Carbon Dioxide Capture. *J. Am. Chem. Soc.* **2011**, *133*, 5664-5667.
16. Chowdhury, P.; Mekala, S.; Dreisbach, F.; Gumma, S., Adsorption of CO, CO₂ and CH₄ on Cu-BTC and MIL-101 Metal Organic Frameworks: Effect of Open Metal Sites and Adsorbate Polarity. *Microporous Mesoporous Mater.* **2012**, *152*, 246-252.
17. Pakseresht, S.; Kazemeini, M.; Akbarnejad, M. M., Equilibrium isotherms for CO, CO₂, CH₄ and C₂H₄ on the 5A molecular sieve by a simple volumetric apparatus. *Sep. Purif. Technol.* **2002**, *28*, 53-60.
18. Sircar, S.; Golden, T. C., Purification of Hydrogen by Pressure Swing Adsorption. *Sep. Sci. and Technol.* **2000**, *35*, 667-687.

19. He, Y.; Xiang, S.; Zhang, Z.; Xiong, S.; Wu, C.; Zhou, W.; Yildirim, T.; Krishna, R.; Chen, B., A microporous metal-organic framework assembled from an aromatic tetracarboxylate for H₂ purification. *J. Mater. Chem. A* **2013**, *1*, 2543-2551.
20. Mohapatra, S.; Hembram, K. P. S. S.; Waghmare, U.; Maji, T. K., Immobilization of Alkali
5 Metal Ions in a 3D Lanthanide-Organic Framework: Selective Sorption and H₂ Storage
Characteristics. *Chem. Mater.* **2009**, *21*, 5406-5412.
21. Maji, T. K.; Mostafa, G.; Chang, H.-C.; Kitagawa, S., Porous lanthanide-organic framework
with zeolite-like topology. *Chem. Commun.* **2005**, 2436-2438.
22. Chandler, B. D.; Yu, J. O.; Cramb, D. T.; Shimizu, G. K. H., Series of Lanthanide-Alkali
10 Metal-Organic Frameworks Exhibiting Luminescence and Permanent Microporosity. *Chem.
Mater.* **2007**, *19*, 4467-4473.
23. Jia, J.; Lin, X.; Blake, A. J.; Champness, N. R.; Hubberstey, P.; Shao, L.; Walker, G.; Wilson,
C.; Schröder, M., Triggered Ligand Release Coupled to Framework Rearrangement:
Generating Crystalline Porous Coordination Materials. *Inorg. Chem.* **2006**, *45*, 8838-8840.
- 15 24. HuanHuan, L.; Zheng, N.; Tian, H.; ZhenJie, Z.; Wei, S.; Peng, C., A microporous lanthanide
metal-organic framework containing channels: Synthesis, structure, gas adsorption and
magnetic properties. *Sci. China Chem.* **2011**, *54*, 1423-1429.
25. Wang, G.; Song, T.; Fan, Y.; Xu, J.; Wang, M.; Wang, L.; Zhang, L.; Wang, L., A porous
lanthanide metal-organic framework with luminescent property, nitrogen gas adsorption and
20 high thermal stability. *Inorg. Chem. Commun.* **2010**, *13*, 95-97.
26. Guo, Z.; Xu, H.; Su, S.; Cai, J.; Dang, S.; Xiang, S.; Qian, G.; Zhang, H.; O'Keeffe, M.; Chen,
B., A robust near infrared luminescent ytterbium metal-organic framework for sensing of small
molecules. *Chem. Commun.* **2011**, *47*, 5551-5553.
27. Xie, L.-H.; Wang, Y.; Liu, X.-M.; Lin, J.-B.; Zhang, J.-P.; Chen, X.-M., Crystallographic
25 studies into the role of exposed rare earth metal ion for guest sorption. *CrystEngComm* **2011**,
13, 5849-5857.
28. Guo, X.; Zhu, G.; Li, Z.; Sun, F.; Yang, Z.; Qiu, S., A lanthanide metal-organic framework
with high thermal stability and available Lewis-acid metal sites. *Chem. Commun.* **2006**,
3172-3174.
- 30 29. Devic, T.; Serre, C.; Audebrand, N.; Marrot, J.; Férey, G., MIL-103, A 3-D Lanthanide-Based
Metal Organic Framework with Large One-Dimensional Tunnels and A High Surface Area. *J.
Am. Chem. Soc.* **2005**, *127*, 12788-12789.

30. Ma, S.; Yuan, D.; Wang, X.-S.; Zhou, H.-C., Microporous Lanthanide Metal-Organic Frameworks Containing Coordinatively Linked Interpenetration: Syntheses, Gas Adsorption Studies, Thermal Stability Analysis, and Photoluminescence Investigation. *Inorg. Chem.* **2009**, *48*, 2072-2077.
- 5 31. Lee, W. R.; Ryu, D. W.; Lee, J. W.; Yoon, J. H.; Koh, E. K.; Hong, C. S., Microporous Lanthanide-Organic Frameworks with Open Metal Sites: Unexpected Sorption Propensity and Multifunctional Properties. *Inorg. Chem.* **2010**, *49*, 4723-4725.
32. Ma, S.; Wang, X.-S.; Yuan, D.; Zhou, H.-C., A Coordinatively Linked Yb Metal-Organic Framework Demonstrates High Thermal Stability and Uncommon Gas-Adsorption Selectivity. *Angew. Chem. Int. Ed.* **2008**, *47*, 4130-4133.
- 10 33. Mu, B.; Li, F.; Huang, Y.; Walton, K. S., Breathing effects of CO₂ adsorption on a flexible 3D lanthanide metal-organic framework. *J. Mater. Chem.* **2012**, *22*, 10172-10178.
34. Jiang, H.-L.; Tsumori, N.; Xu, Q., A Series of (6,6)-Connected Porous Lanthanide-Organic Framework Enantiomers with High Thermostability and Exposed Metal Sites: Scalable Syntheses, Structures, and Sorption Properties. *Inorg. Chem.* **2010**, *49*, 10001-10006.
- 15 35. Park, Y. K.; Choi, S. B.; Kim, H.; Kim, K.; Won, B.-H.; Choi, K.; Choi, J.-S.; Ahn, W.-S.; Won, N.; Kim, S.; Jung, D. H.; Choi, S.-H.; Kim, G.-H.; Cha, S.-S.; Jhon, Y. H.; Yang, J. K.; Kim, J., Crystal Structure and Guest Uptake of a Mesoporous Metal-Organic Framework Containing Cages of 3.9 and 4.7 nm in Diameter. *Angew. Chem. Int. Ed.* **2007**, *46*, 8230-8233.